Future Circular Collider

PUBLICATION

Material options for the superconducting rf system of the Future Circular Collider

Aull, Sarah () *et al.*

21 June 2018

The research leading to this document is part of the Future Circular Collider Study

The electronic version of this FCC Publication is available
on the CERN Document Server at the following URL :
<http://cds.cern.ch/record/2625126>

Material Options for the Superconducting RF System of the Future Circular Collider

S. Aull* and O. Brunner, A. Butterworth, N. Schwerg
CERN, Geneva, Switzerland
(Dated: April 18, 2017)

The design of the superconducting RF (SRF) systems of the Future Circular Collider (FCC) machine variants requires a thorough comparison of the different options for cavity material, operating temperature and frequency. We collected representative SRF performance data at different frequencies and temperatures of bulk niobium as the standard technology and of niobium thin films as a potential alternative and develop a perspective for future performance for all material-frequency-temperature combinations as function of accelerating gradient. Based on this perspective, we estimate the corresponding cryogenic grid power for the different FCC machines showing the most favourable accelerating gradients for the different materials and operating temperatures. Furthermore, we discuss advantages, disadvantages and limitations of the different technology options to be taken into consideration.

CONTENTS

I. INTRODUCTION ON RF REQUIREMENTS OF FCC

The definition and optimization of the radio-frequency (RF) system of the Future Circular Collider (FCC) is an important item of the machine study [1]. Its parameter space is constrained by the FCC-hh and -ee machines' parameters at the various centre-of-mass energies (Z peak, WW threshold, HZ cross-section maximum, and top-pair threshold) [2]. In view of the fact that it is not optimal to make one RF configuration cover all options, two baseline scenarios are considered. The first is an *ampere-class* operating scenario for the FCC-hh, Z peak and WW threshold parameters, which demands low frequency, low shunt resistance cavities, low number of cells and high RF power per cell. For this scenario a 400 MHz continuous wave (CW) RF system made up of 32/50 single cell cavities per beam is considered (resp. for -hh / Z peak), with an RF power per cavity of the order of 1 MW. The WW threshold energy will then be reached by adding a few tens of two-cell cavities. This frequency is the natural choice for the FCC-hh, which will profit from LHC as injector, and offers good perspectives for the FCC-ee low energy machines. A second operating scenario is considered for the H and $t\bar{t}$ threshold operation points where high acceleration efficiency and multi-cell cavities are required to optimize the total size of the RF system. About 2600 cells are needed to produce the total RF voltage (10 GV) of the highest energy point. Due to the lower beam loading, both 400 MHz and 800 MHz are considered, but higher frequencies have been eliminated due to transverse impedance considerations and power coupler limitation in CW. In the following we describe and justify the different material options for the two scenarios.

TABLE I. Salient Machine Parameters for FCC-ee [3]

	Z	Z2	W	H	$t\bar{t}$
Beam energy in GeV	45.6		80	120	175
Beam current in mA	1450		152	30	6.6
Total RF voltage V_{RF} in GV	0.4	0.2	0.8	3	10

II. SRF MATERIAL OPTIONS

The surface resistance R_S of any SRF material can be described as the sum of a contribution from the BCS theory of superconductivity R_{BCS}, a residual part R_{res} and a non-linear part R_{nl}:

$$R_S = R_{BCS} + R_{res} + R_{nl}. \quad (1)$$

* sarah.aull@cern.ch

For a clean superconductor, R_{BCS} depends on frequency f, operating temperature T, critical temperature T_{c} and the residual resistance ratio RRR of the material as

$$R_{\mathrm{BCS}} \sim f^2 \exp\left(T/T_{\mathrm{c}}\right) \cdot \mathrm{RRR}. \tag{2}$$

The residual resistance, R_{res}, is temperature independent and depends only slightly on frequency [4] so that R_{res} is considered to be constant over all frequencies. Due to the exponential dependence on temperature of R_{BCS}, the BCS resistance is the dominant contribution at 4.2 K while the residual resistance dominates the total surface resistance at 2 K. The non-linear resistance R_{nl} describes the surface resistance as a function of RF field and might additionally depend on temperature and/or frequency.

In the following we review the current and future performance of the different available material options for FCC. For each material we present recent measurements and discuss the effect of future improvements providing a material baseline for design studies and comparisons of the different FCC variants.

Any baseline $R_{\mathrm{S,baseline}}$ will be described through the presented surface resistance data $R_{\mathrm{S,\,data}}$, the difference between measured residual resistance and expected series production residual resistance (ΔR_{res}) and additional BCS contribution (ΔR_{BCS}) due to the fact that the accelerator may run at 4.5 K and measurements are usually done between 4.0 K and 4.2 K:

$$R_{\mathrm{S,baseline}} = R_{\mathrm{S,data}} - \Delta R_{\mathrm{res}} + \Delta R_{\mathrm{BCS}}. \tag{3}$$

The difference in BCS resistance is calculated using the Winsuperfit code using standard material parameters [5]. Note that the surface resistance data is plotted versus peak surface magnetic induction B_{pk} to allow for a simple and cavity independent comparison.

Bulk Niobium

Bulk niobium is the standard material for superconducting RF cavities. There is great experience and a high level of expertise in terms of fabrication, processing and operation of bulk niobium cavities in industry as well as in research laboratories around the world. However, the cost for high quality material is significant and additional costs for magnetic shielding arise. Typically, bulk niobium cavities require a magnetic shielding down to less than 1 micro tesla which is especially challenging for large accelerating structures like low frequency and/or multicell cavities. In order to thermally stabilize a cavity, the raw material has to have a RRR value of at least 300 which increases the BCS losses significantly as can be seen from Equation 2. Moreover, bulk niobium cavities favour operation in the superfluid helium regime (≤ 2.1 K) due to the limited thermal conductivity of Helium I.

In general the bulk niobium technology can be considered as mastered. We therefore expect significant improvements only in the context of surface preparation, assembly and mass production techniques rather than on the material performance side.

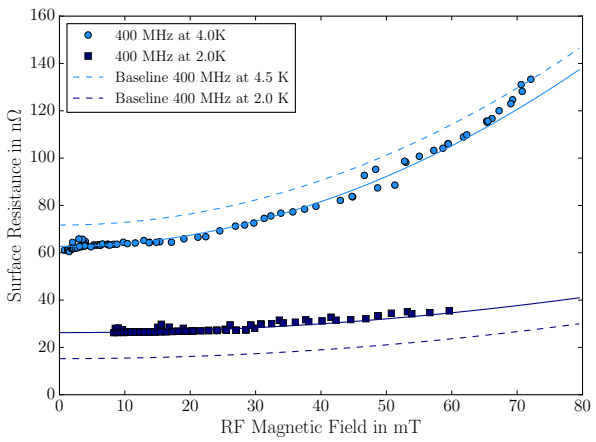

FIG. 1. Surface Resistance of a bulk niobium crab cavity at 400 MHz with quadratic fit. The expected performance of an elliptical bulk niobium cavity with standard residual resistance and corrections for additional BCS losses at 4.5 K is indicated as dashed lines. Data courtesy of K. Hernandez-Chahin et al. [6].

Bulk Niobium at 400 MHz

Figure 1 shows the typical RF performance of bulk niobium at 400 MHz, measured on the *double quarter wave* crab cavity at CERN [6]. The measurement error is in the order of 10 %.

We assume that the performance of the crab cavity is a reasonable reference although a simpler geometry like an elliptical cavity is easier to prepare in terms of surface preparation and cleaning. The better performance of an elliptical cavity may be compensated by a greater surface area compared to the crab cavity with the inherent increased risk of performance degrading or limiting defects. Both surface resistance curves are fitted with a quadratic magnetic field dependency and a zero-rf-field component; the resulting fit parameters ($\pm$ one standard deviation) can be found in Table II.

For setting a baseline performance for bulk niobium at 400 MHz and 2.0 K, the residual resistance is matched to 15 nΩ at zero field which we consider realistic for a cavity in series production. For the 4.5 K baseline, an additional offset is introduced to account for the additional BCS contribution between 4.0 K and 4.5 K. The Q-slope, i.e. the increase of surface resistance with field, is preserved for both temperatures. Both baselines are indicated in Figure 1 as dashed lines. Note that, in the case of the 4.5 K baseline, the scaling from 4 to 4.5 K outweighs the effect of the reduced residual contribution.

TABLE II. Fit parameters for bulk Nb data at 400 MHz. Data and fits are shown in Figure 1.

	fit function	a in 10^{-3}nΩ/(mT)^2	b in nΩ
2.0 K	$a \cdot B_{\mathrm{pk}}^2 + b$	(2.3 ± 0.2)	(26.24 ± 0.08)
4.0 K		(11.81 ± 0.10)	(62.69 ± 0.08)

Bulk Niobium at 800 MHz

For a projection of the performance of a bulk niobium cavity at 800 MHz we use recent results on a 704 MHz 5-cell cavity from CERN's high gradient programme as reference [7]. The measurement error is in the order of 10 %. The 4 K data follows the typical quadratic trend and shows strong surface resistance increase with field. The 2 K data increases only minimally with field and shows a linear dependence on the RF field. The data and according fits are shown in Figure 2 while the fit parameters can be found in Table III.

For the baseline performance estimate, the residual resistance is matched to 15 nΩ for both temperatures and an additional BCS contribution to account for 4.5 K instead of 4.1 K is added. To account for the slightly higher frequency, the Q-slope is scaled quadratically with frequency. The resulting baseline for 800 MHz is shown in Figure 2 as dashed lines. Note that, in the case of the 4.5 K baseline, the scaling from 4.1 K to 4.5 K outweighs the effect of the reduced residual contribution while for the 2 K data differences are negligible.

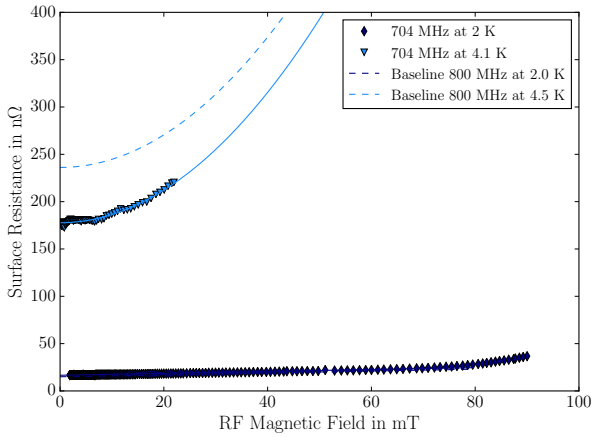

FIG. 2. Surface Resistance of a bulk niobium *high gradient* cavity at 704 MHz with linear (2 K) and quadratic (4.2 K) fits as solid lines. The expected performance of a bulk niobium cavity at 800 MHz with standard residual resistance and corrections for additional BCS losses at 4.5 K is indicated with dashed lines. Data courtesy of A. Macpherson et al. [7].

TABLE III. Fit parameters for bulk Nb data at 704 MHz. Data and fits are shown in Figure 2.

	fit function	a	b in nΩ
2.0 K	$a \cdot B_{\mathrm{pk}} + b$	(0.10 ± 0.01) nΩ/mT	(16.6 ± 0.2)
4.1 K	$a \cdot B_{\mathrm{pk}}^2 + b$	$(86.1 \pm 0.1)\, 10^{-3}$nΩ/(mT)^2	(177.7 ± 0.1)

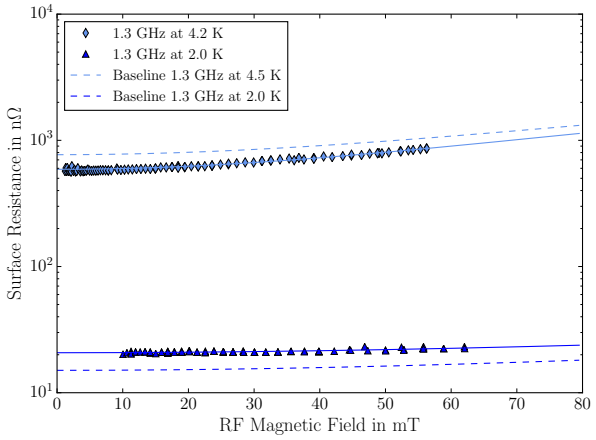

FIG. 3. Surface Resistance of a bulk niobium cavity at 1.3 GHz as well as the expected performances with standard residual resistance at 2.0 K.

Bulk Niobium at 1.3 GHz

Figure 3 shows the typical RF performance of a 1.3 GHz (single cell) bulk niobium cavity at 2 K and 4.2 K. Note that due to the high BCS part the plot is on a logarithmic scale. The measurement error is in the order of 10 %. Both surface resistance curves can be fitted with a quadratic magnetic field dependency, and the resulting fit parameters can be found in Table IV.

For setting a baseline performance for bulk niobium at 1.3 GHz, the residual resistance is again matched to 15 nΩ for both temperatures. For the 4.5 K baseline, an additional offset is introduced to account for the additional BCS contribution between 4.2 K and 4.5 K. The Q-slope, i.e., the increase of surface resistance with field is preserved for both temperatures. Both baselines are indicated in Figure 3 as dashed lines. Note that, in the case of the 4.5 K-baseline, the scaling from 4.2 K to 4.5 K outweighs the effect of the reduced residual resistance.

TABLE IV. Fit parameters for bulk Nb data at 1.3 GHz. Data and fits are shown in Figure 3

	fit function	a in 10^{-3}nΩ/(mT)^2	b in nΩ
2.0 K	$a \cdot B_{\mathrm{pk}}^2 + b$	(0.48 ± 0.03)	(20.74 ± 0.04)
4.0 K		(0.86 ± 0.01)	(589.2 ± 1.5)

Nitrogen Doping

Nitrogen doping is a post-processing technique for bulk niobium cavities where nitrogen is diffused into the surface layer during a high temperature bakeout [8]. This nitrogen treatment shortens the mean free path and prevents nano-hydrides from forming during cool down which eventually results in a minimized BCS resistance and therefore higher Q_0 [9]. N doped cavities are still

to be operated below 2.1 K where the BCS resistance is small even at 1.3 GHz. Due to the fact that all N doping studies have been done on 1.3 GHz cavities and at 2.0 K, the behaviour at other frequencies and/or temperatures is difficult to estimate. When going to lower frequencies, we expect the effect to be less pronounced as the BCS resistance scales with the square of the frequency. At 400 MHz as well as 800 MHz and at 2.0 K an optimization of the BCS resistance is expected to achieve a gain of the order of 2 nΩ. A positive effect of N doping on the residual resistance was also reported but smaller than the gain in BCS resistance [9].

For a quantitative estimate low frequency data as well as data at 4.2 K are necessary and a deeper understanding of the effect on the residual resistance is required. Moreover, N doped cavities show a stronger sensitivity to losses from trapped magnetic flux [9] which already resulted in tighter magnetic shielding requirements in LCLS-II [10].

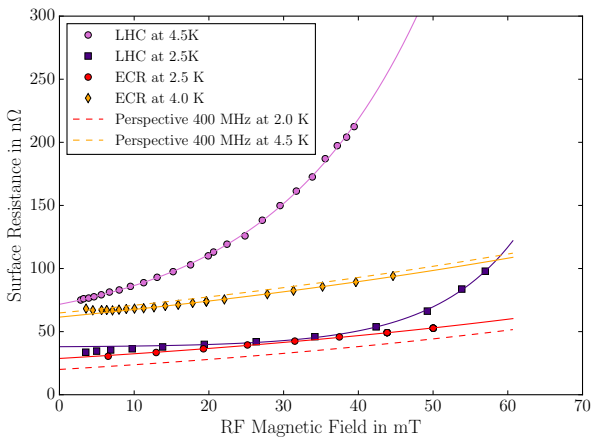

FIG. 4. Surface Resistance of a standard LHC cavity [16] and a Nb/Cu film sample [17] at 400 MHz and the expected performance of an elliptical Nb/Cu cavity with standard residual resistance and corrections for additional BCS losses at 4.5 K.

Niobium Thin Films

The SRF thin film technology is based on decoupling the RF surface from the cavity geometry with its thermomechanical requirements. CERN has a long history of sputter-coating copper cavities with a 1 µm to 2 µm thick niobium film which have been used in the LEP machine and are currently in operation in the LHC and HIE-Isolde [11–13]. The main advantages of this technology are the thermal stability due to the high thermal conductivity of the copper, the reduced raw material cost and the fact that Nb/Cu cavities do not suffer from losses due to trapped magnetic field and therefore do not need magnetic shielding in the accelerator. However, Nb/Cu cavities show significantly stronger RF field dependent losses compared to bulk niobium (*Q-slope*) which limits to date their application to about 10 MV/m (in elliptical geometries) [14]. Different new coating techniques, so called energetic condensation techniques, are currently under development in different laboratories around the world. These new techniques promise to improve the microstructure of the niobium thin film and are expected to improve the SRF performance of these films significantly [15].

Nb/Cu at 400 MHz

A typical LHC performance curve at 2.5 K and 4.5 K is shown in Figure 4 as adapted from [16]. The characteristic Nb/Cu *Q*-slope is clearly visible already for moderate fields. Figure 4 also shows the first surface resistance measurement of a Nb/Cu film coated using *electron-cyclotron-resonance* (ECR) [17, 19]. The ECR technique is one representative of the energetic condensation techniques and currently pursued by Jefferson Lab. It has to be noted however that this film was deposited on a flat sample and characterized with the Quadrupole Resonator at CERN [20]. This technique has not been transferred to 3D geometries yet. Nonetheless, a strong mitigation of the *Q*-slope is evident and a similar performance is expected on elliptical cavities. The key advantage of the energetic condensation techniques is the fact that the niobium is ionized and not deposited as neutrals as is the case for the standard sputtering. The ions can be guided via magnetic and electric fields so that the resulting microstructure is significantly less dependent on the incident angle of the arriving particle [21].

Despite the improved performance, the ECR film nevertheless shows an exponential increase of surface resistance with RF field. In analogy to the bulk niobium data, the perspective for Nb/Cu performance is based on fitting the (ECR) data which can be found in Table V and the residual resistance and BCS contribution are adjusted. Although Nb/Cu cavities have been demonstrated to reach very low residual resistances [14], we set 20 nΩ at 2 K as a residual resistance in series production and account for the changes in the BCS contribution as a constant offset. As previously, the field dependence is preserved.

TABLE V. Fit parameters for the ECR Nb/Cu data at 400 MHz. Data and fits are shown in Figure 4.

	fit function	a in nΩ	b in 10^{-3}/mT
2.5 K	$a \cdot \exp\left(b \cdot B_{\mathrm{pk}}\right)$	(28.73 ± 0.17)	(12.2 ± 0.1)
4.0 K		(61.51 ± 0.19)	(9.41 ± 0.08)

Nb/Cu at 800 MHz

Figure 5 shows the surface resistance measured at 800 MHz of the same ECR coating which also provided the 400 MHz data. There are no Nb/Cu cavities at or close to 800 MHz, so this data set must serve as the only

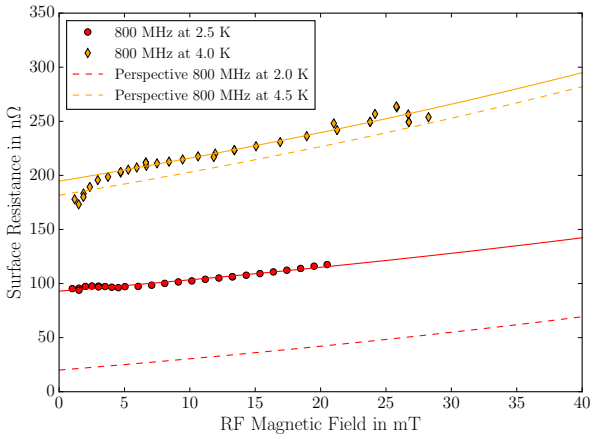

FIG. 5. Surface Resistance of a Nb/Cu film sample at 800 MHz [18] and the expected performance of an elliptical Nb/Cu cavity with standard residual resistance and corrections for additional BCS losses at 4.5 K.

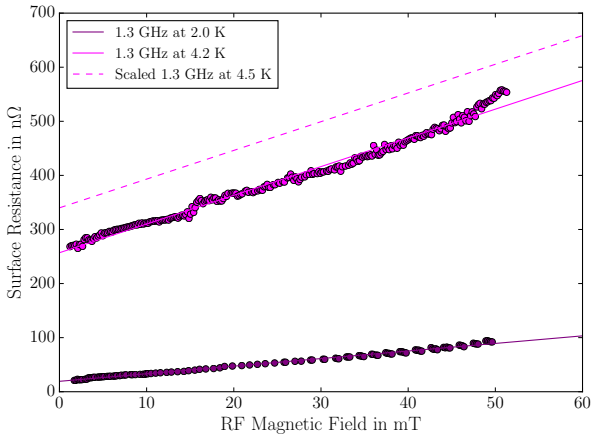

FIG. 6. Surface Resistance of a Nb/Cu cavity at 1.3 GHz as well as the expected performances with standard residual resistance and BCS corrections [22].

TABLE VI. Fit parameters for Nb/Cu data at 800 MHz. Data and fits are shown in Figure 5.

	fit function	a in nΩ	b in 10^{-3}/mT
2.5 K	$a \cdot \exp\left(b \cdot B_{\mathrm{pk}}\right)$	(93.0 ± 0.4)	(10.6 ± 0.4)
4.0 K		(194.6 ± 3.5)	(10.4 ± 0.8)

data available. The data is again fitted exponentially, matched to a residual resistance of 20 nΩ and an offset is introduced to account for additional BCS losses. The fit parameters can be found in Table VI.

Nb/Cu at 1.3 GHz

The baseline for Nb/Cu performance at 1.3 GHz is based on the *high impulse power magnetron sputtering* (HIPIMS) R&D programme at CERN. The data shown in Figure 6 is currently the best HIPIMS cavity [22]. The surface resistance increase with field is linear for both temperatures. The 2.0 K data only needs a small adjustment to match 20 nΩ residual resistance. For the 4.5 K baseline performance an offset to account for additional BCS losses is added to the RF data at 4.2 K. The offset is determined by fitting the surface resistance data as a function of temperature between 2.0 K and 4.2 K and extrapolating to 4.5 K. The fit parameters can be found in Table VII and the baselines are indicated in Figure 6.

TABLE VII. Fit parameters for Nb/Cu data at 1.3 GHz. Data and fits are shown in Figure 6.

	fit function	a in nΩ/mT	b in nΩ
2.0 K	$a \cdot B_{\mathrm{pk}} + b$	(1.40 ± 0.01)	(19.2 ± 0.3)
4.2 K		(5.31 ± 0.04)	(257.0 ± 1.1)

Niobium-Tin

Niobium-Tin (Nb_3Sn) is the most advanced material for SRF applications beyond niobium. The higher critical temperature and the higher superheating field promise low cryogenic consumption at 4.5 K and accelerating gradients beyond 50 MV/m [25]. So far, individual 1.3 GHz single cell cavities from bulk niobium have been repeatedly coated with Nb_3Sn through an evaporation deposition method reaching Q_0 values of 10^{10} at 4.2 K but all cavities are currently limited below 18 MV/m [23, 24]. Although Nb_3Sn will certainly play a big role in future accelerators, for now, it has to be acknowledged that this is not yet a mature technology. A better understanding and improvement of the quench fields is required and experience with dressed cavities, tuner operation and magnetic field requirements need to be gained.

III. MATERIAL-MACHINE CONSIDERATIONS

The design of the RF system for an accelerator depends on a number of design variables, interdependent quantities and limitations. The choice of one of the materials above influences the overall power consumption of the machine, the length of the RF installation and the production effort for the cavities [28].

Cryogenic Losses

For a machine, simply specified by the required accelerating voltage V_{RF} (see Tab. I), we study the overall refrigeration power for the different material, frequency and temperature combinations.

Any power dissipated into the helium, $P_{\mathrm{dissipated}}$, has

to be scaled with the Carnot efficiency,

$$\eta_{\mathrm{carnot}} = \frac{T}{T_{\mathrm{amb}} - T}, \tag{4}$$

with the ambient temperature $T_{\mathrm{amb}} = 295\,\mathrm{K}$ and the operation temperature T. The technical efficiency of the cryogenic plant is estimated with $\eta_{\mathrm{tech}} = 20\,\%$ for 2 K operation and $\eta_{\mathrm{tech}} = 30\,\%$ for 4.5 K operation [29] in order to compute the required refrigeration power $P_{\mathrm{refrigeration}}$ drawn from the power grid:

$$P_{\mathrm{refrigeration}} = \frac{P_{\mathrm{dissipated}}}{\eta_{\mathrm{carnot}}\eta_{\mathrm{tech}}}. \tag{5}$$

The total power consumption for the cryogenic system, P_{cryo}, is the sum of the static losses P_{static} and the dynamic losses P_{dynamic} scaled to ambient temperature.

$$P_{\mathrm{cryo}} = \frac{P_{\mathrm{static}} + P_{\mathrm{dynamic}}}{\eta_{\mathrm{carnot}}\eta_{\mathrm{tech}}}. \tag{6}$$

The static losses per unit lenght, $P'_{\mathrm{static}} = 5\,\mathrm{W/m}$, are estimated with 5 W/m which is less than for the LEP cavities (8 W/m [11]) but still relaxed compared to the static losses of the LHC dipole magnets (0.2 W/m [12]). The static losses are also a function of the number of cavities per cryomodule and the number of fundamental power and HOM couplers, both disregarded for this estimation.

The length of the cold section(s) is given by the length of the cavity cells $n_{\mathrm{cell}}\ell_{\mathrm{cell}}$ (with $\ell_{\mathrm{cell}} \approx \lambda_{\mathrm{RF}}/2$) plus a fixed length for the beam tubes of 50 cm on each side of each cavity, and by the total number of cavities needed to provide total RF voltage V_{RF} for a given accelerating gradient,

$$n_{\mathrm{cavity}} = \frac{V_{\mathrm{RF}}}{E_{\mathrm{acc}} n_{\mathrm{cell}} \ell_{\mathrm{cell}}}. \tag{7}$$

The static heat losses are then:

$$P_{\mathrm{static}} = P'_{\mathrm{static}} \cdot n_{\mathrm{cavity}} \cdot (n_{\mathrm{cell}}\ell_{\mathrm{cell}} + 1\,\mathrm{m})\,. \tag{8}$$

The dynamic losses in each superconducting cell scale quadratically with the accelerating voltage $V_{\mathrm{acc}} = l_{\mathrm{cell}} E_{\mathrm{acc}}$ and depend additionally on the surface resistance of the material R_{S} and on the geometry of the cavity cell which has an influence on the R/Q and the geometry factor G. The dynamic heat losses are accordingly:

$$P_{\mathrm{dynamic}} = n_{\mathrm{cavity}} n_{\mathrm{cell}} \frac{\left(E_{\mathrm{acc}} \cdot \ell_{\mathrm{cell}}\right)^2}{R/Q \cdot G} R_{\mathrm{S}}. \tag{9}$$

For all calculations we will use a geometry factor of 280 Ω and an R/Q of 85 Ω per cell (circular notation).

Figure 7 displays schematically the static, dynamic and total cryogenic losses as function of accelerating gradient. With increasing accelerating gradient, the machine becomes shorter and the static losses decrease. In contrast, the dynamic losses increase linearly with accelerating gradient E_{acc} since the number of cells n_{cell} times cavities n_{cavity} in Equation 9 decreases with $1/E_{\mathrm{acc}}$ for a given total RF voltage. The slope of the dynamic loss increase is mainly given by the surface resistance of the material at the operating conditions (frequency, temperature, RF field).

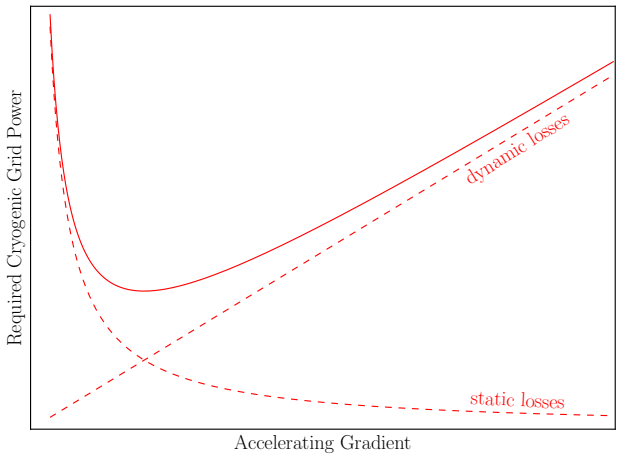

FIG. 7. Static, dynamic and total heat load as function of accelerating gradient. Position of the minimum depends and steepness of the dynamic losses depend on the surface resistance.

The total cryogenic consumption has an optimum accelerating gradient where the total cryogenic losses are minimal. This optimum accelerating gradient depends predominantly on the surface resistance and on the length of the installation. The length of the RF installation decreases with increasing number of cells per cavity and the optimum accelerating gradient decreases accordingly. Figure 8 plots the optimum accelerating gradient as a function of surface resistance and for 400 MHz, 800 MHz and 1.3 GHz single cell cavities as upper limit as the optimum gradient shifts towards lower values with increasing number of cavity cells. The optimum accelerating gradient is also shown for a 1.3 GHz 9-cell cavity for comparison. It can be concluded that accelerating gradients well below 30 MV/m will be sufficient for most accelerator projects as long as restrictions on the installation length are not too tight.

In general the accelerating gradient is the dominant design choice in terms of cryogenic power consumption: The total RF voltage is given by the machine parameters while the geometry related quantities R/Q and G can be optimized within the order of 10 %. The surface resistance on the other hand is a consequence of material choice, frequency, operating temperature and RF magnetic field (which is proportional to the accelerating gradient).

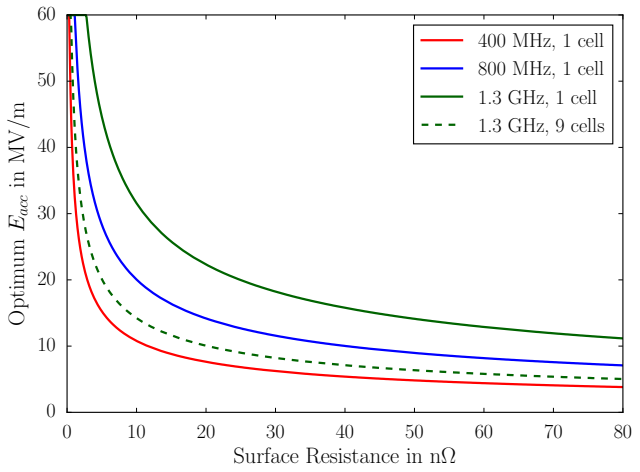

FIG. 8. Optimum accelerating gradient for minimal total cryogenic power consumption as function of surface resistance for a static heat load of 5 W/m.

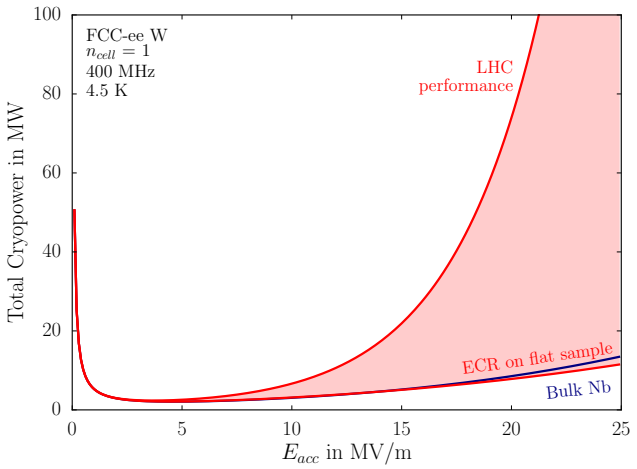

FIG. 9. FCC-ee W: Total cryogenic consumption as function of accelerating gradient for Nb/Cu and bulk Nb both at 400 MHz and 4.5 K. Other frequency/temperature options are discarded due to other factors.

Cryogenic Losses for FCC-ee

The baseline performances for each material-frequency-temperature combination as function of RF field can now be used to estimate the corresponding required grid power for the cryogenic system using Equations 8 and 9. In addition, taking restrictions on the RF system such as beam dynamics, technology limits or available space into account, the favourable material-frequency-temperature option(s) with a reasonable range for the accelerating gradient can be derived for each FCC machine scenario.

FCC-ee Z and W

The first two FCC-ee stages on the Z and the W pole are characterized by low energy but extremely high beam current and should share the same RF system. The main issues for the RF system will be handling relatively high *higher order mode* (HOM) losses and providing high power to the cavities. The maximum power limit of the fundamental power coupler restricts the operation of the cavities to lower accelerating gradients and the high HOM loads favour 400 MHz single cell cavities and 4.5 K operation.

In terms of cryogenics, the W machine will have the highest consumption among the ampere-class machines and will therefore serve here as the base for discussing the material options in terms of cryogenic power. Figure 9 compares the required cryogenic grid power for bulk niobium and Nb/Cu for 400 MHz and 4.5 K. The typical LHC performance is indicated as well as the demonstrated performance of the ECR film sample. The coloured area between the two is the gain which we expect from further thin film R&D on the energetic condensation techniques.

Considering that these cavities will need to be operated in the order of 5 MV/m to 10 MV/m, it can be concluded that Nb/Cu and bulk Nb will have comparable cryogenic consumption and the decision on the material needs consideration of the difference in cost of the complete cryomodule.

FCC-ee H and $t\bar{t}$

The FCC machines on the Higgs and top pole are characterized by high energy and more manageable beam current with less constraints on HOM loads and fundamental power couplers. The high RF voltages favour high(er) accelerating gradients with regard to the length of the RF installation. In the same context, it is worth mentioning that when comparing different frequencies, the active length per cell changes accordingly. Compensation of the shorter active length of higher frequency cavities can be done either through a higher number of cells per cavity or by increasing the accelerating gradient. The maximum number of cells per cavity is subject to an ongoing study [26, 27]. Considering the risk of HOM build-up and related instabilities, we focus on the case of 4-cell cavities. A higher or lower number of cells per cavity changes the cryogenic consumption only slightly as only the static losses are affected. The general conclusions remain therefore valid.

We discard the 1.3 GHz options because of power coupler limitations in CW and transverse impedance considerations.

Figure 10 shows the required cryogenic grid power of all remaining options combining 400 MHz/800 MHz, 2 K/4.5 K, Nb/Cu and bulk Nb. The colored area indicates again the reach of Nb/Cu R&D with the performance of the ECR sample as mid-term goal. All other Nb/Cu lines are already the performance perspective in-

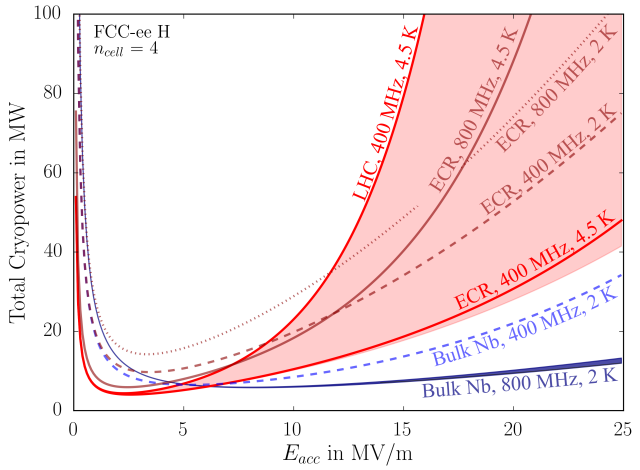

FIG. 10. FCC-ee H: Total cryogenic consumption as function of accelerating gradient for 400 MHz Nb/Cu at 4.5 K compared to 800 MHz bulk Nb at 2.0 K.

cluding the R&D as discussed in Section II.

Comparing the mid-term expected performances of the Nb/Cu options, it can be seen that the 400 MHz, 4.5 K option is the strongest one as it is comparable with the bulk Nb performance at the same frequency and temperature [19]. Nonetheless, on a long-term perspective, the new coating techniques promise to approach the bulk niobium performances also for lower temperature and higher frequencies.

Comparing the bulk niobium options, the 800 MHz option appears stronger than the 400 MHz despite the fact that at 2 K the frequency dependent BCS contribution is negligible. We assume that this difference is due to more experience in the production of higher frequency and in particular elliptical cavities compared to non-elliptical shapes.

Comparing now the two materials, Nb/Cu at 400 MHz, 4.5 K and 10 MV/m has similar cryogenic power consumption to a bulk Nb system at 800 MHz, 2 K and 20 MV/m. In this example, doubling the accelerating gradient for the 800 MHz option compensates for the shorter active length so that the total number of cavities is the same for both systems. Nonetheless, the RF installation will be longer by about 30 % for the 400 MHz option but still far below the limit [28]. The optimal accelerating gradient for both options needs to take into account the production cost of the cryomodules as well. From a cryogenic consumption point of view, a lower $E_{\rm acc}$ would be beneficial, but is counteracted by a higher number of cavities and cryomodules.

The parameters of the two competing cavity options for the FCC-ee Higgs machine are summarized in Table VIII.

The general assumptions of the H machine remain valid for the $t\bar{t}$ machine so that Figure 11 shows only the two remaining options: Nb/Cu at 400 MHz and 4.5 K and bulk Nb at 800 MHz and 2 K. As for the Higgs machine, we find two working points, 10 MV/m for the Nb/Cu option and 20 MV/m for the bulk Nb option, with (almost) the same cryogenic consumption. The RF installation of the 400 MHz system would be about 36 % longer but is also still well below the limit of 6 km [28]. Note that for the $t\bar{t}$ machine the counter rotating beams will share the same accelerating cavities. The parameters of the two competing options for the FCC-ee $t\bar{t}$ machine are summarized in Table IX.

TABLE VIII. Competing cavity options for FCC-ee H per beam.

	Nb/Cu	Bulk Nb
Number of cells per cavity	4	
Required cryogenic power	10 MW	9 MW
Frequency	400 MHz	800 MHz
Operating temperature	4.5 K	2 K
Accelerating gradient	10 MV/m	20 MV/m
Total number of cavities	200	
RF installation length	500 m	350 m

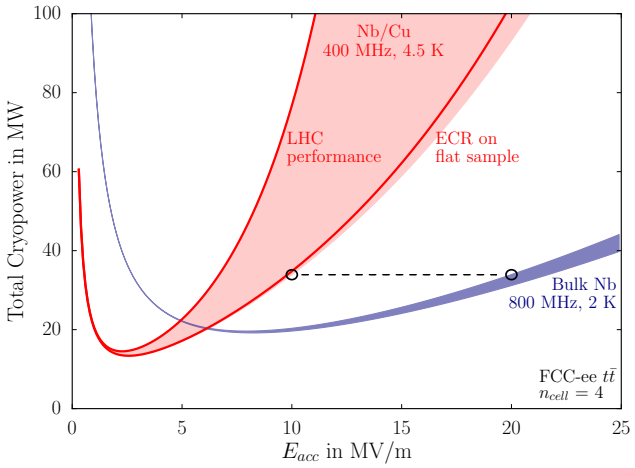

FIG. 11. FCC-ee $t\bar{t}$: Total cryogenic consumption as function of accelerating gradient for 400 MHz Nb/Cu at 4.5 K compared to 800 MHz bulk Nb at 2.0 K.

TABLE IX. Competing cavity options for FCC-ee $t\bar{t}$ where both beams share the RF system.

	Nb/Cu	Bulk Nb
Number of cells per cavity	4	
Required cryogenic power	34 MW	32 MW
Frequency	400 MHz	800 MHz
Operating temperature	4.5 K	2 K
Accelerating gradient	10 MV/m	20 MV/m
Total number of cavities	889	
RF installation length	1.9 km	1.4 km

IV. ADDITIONAL CONSIDERATIONS

While the quality factor of the cavities is the cost driver in terms of dynamic cryogenic losses, other factors may be considered to lower installation cost and RF power consumption. High quality copper as it is used for cavity substrates only costs a fraction of high grade bulk niobium and is less expensive in terms of chemical surface preparation while high pressure water rinsing and clean room assembly are similar. Moreover, the high thermal conductivity of the copper ensures thermal stability even for thicker cavity walls. Increasing the thickness of the cavity wall increases in turn the mechanical stability which reduces microphonics and therefore requires less RF power for the feedback system.

In addition, Nb/Cu cavities have been shown to have very low trapped flux sensitivity throughout the entire SRF cavity frequency range [14]. Trapped magnetic flux is ambient magnetic field that is not expelled at the transition to the Meissner state of the niobium but pinned at imperfections such as grain boundaries or lattice defects. Each magnetic flux line has a normal conducting core which oscillates under the influence of the RF and adds to the residual resistance. The residual resistance increase for bulk Nb is typically of the order of $3\,\mathrm{n\Omega/\mu T}$ and easily a factor of 3 more for N doped cavities. In contrast, Nb/Cu cavities have trapped flux sensitivities of the order of $0.03\,\mathrm{n\Omega/\mu T}$. For a cryomodule without any shielding of the earth magnetic field (about $50\,\mu\mathrm{T}$), the residual resistance would increase by about $150\,\mathrm{n\Omega}$ for bulk Nb and less than $2\,\mathrm{n\Omega}$ for Nb/Cu. As a consequence, cavities made from bulk niobium require magnetic field shielding down to typically $0.5\,\mu\mathrm{T}$ which can only be achieved by warm and cold shields. Cryomodules with Nb/Cu cavities do not have any magnetic shielding ([11–13]) which not only reduces the cost but also eases the cryomodule design.

In terms of cryogenics a 2 K system is 2 to 3 times more complex and more cost intensive (per kW) than a 4.5 K system [29].

From a beam dynamics point of view, more detailed studies are necessary to find the optimum number of cells and an optimum frequency. Frequencies (slightly) below 400 MHz operated at 4.5 K should result in slightly better performance due to the lower BCS resistance. Frequencies significantly higher than 400 MHz require 2 K operation due to the quadratic increase of BCS resistance with frequency and exponential increase with temperature. Extending the application range of Nb/Cu to 2 K and higher frequency will require further development effort.

In contrast bulk Nb cavities of lower frequency will increase the material cost, but is beneficial in terms of accelerating voltage per cell. Higher frequency cavities will be smaller, but require an increase of the total number of cavities or of the accelerating gradient (and hence cryogenic consumption) and will suffer more from HOM losses.

V. CONCLUSION

We collected representative SRF performance data of different RF frequencies, temperatures and materials and developed a performance perspective from future R&D. With this baseline, we estimated the required grid power for the cryogenic system of each frequency-temperature-material combination as function of RF field and presented the valid options for all FCC-ee machines. The low energy-extremely high current machines strongly favour 400 MHz single cell cavities operated at 4.5 K and low accelerating gradient. For such application, the Nb/Cu technology is already the strongest candidate. For the high energy machines, the Nb/Cu technology is competitive with bulk Nb provided the current R&D efforts are further pursued. Improving the performance of the Nb/Cu technology to an extent that cryogenic losses are comparable to the bulk niobium technology would allow to profit from the advantages of Nb/Cu cavities in terms of production cost and simpler cryomodule design.

A thorough cost estimate considering cavity and cryomodule production, cryogenic installation and RF power system is required in addition to the beam dynamics considerations to take a decision between the two competing technologies.

[1] M. Benedikt and F. Zimmermann, *Future Circular Colliders*, CERN-ACC-2015-0164, 2015.

[2] The TLEP Design Study Working Group *First Look at the Physics Case of TLEP*, arXiv:1308.6176 [hep-ex] (2014).

[3] F. Zimmermann et al., *Future Circular Collider Study Lepton Collider Parameters*, EDMS 1346081 V.3 (2016).

[4] G. Ciovati et al., *Residual Resistance Data From Cavity Production Projects at Jefferson Lab*, IEEE T Appl Supercon 21, 1914 - 1917 (2011).

[5] G. Ciovati, *SUPERFIT: a Computer Code to Fit Surface Resistance and Penetration Depth of a Superconductor*, Technical Note TN-03-003, Jefferson Lab, 2003.

[6] K. Hernandez-Chahin, et al., *Performance Evaluation of HL-LHC Crab Cavity Prototypes in a CERN Vertical Test Cryostat*, THPB050, SRF 2015.

[7] A. Macpherson, et al., *CERN's Bulk Niobium High Gradient SRF Programme: Developments and Recent Cold Test Results*, MOPB074, SRF 2015.

[8] A. Grassellino et al., *Nitrogen and Argon doping of Niobium for Superconducting Radio Frequency Cavities: a Pathway to Highly Efficient Accelerating Structures.* Superconductor Science and Technology 26, 102001 (2013).

[9] A. Grassellino, *N Doping: Progress in Development and Understanding*, MOBA06, SRF 2015.

[10] S.K. Chandrasekaran, *LCLS-II CM Ambient Magnetic Field Management*, TTC Meeting, Saclay, 2016.

[11] *LEP design report, V.3: LEP2*, CERN-AC-96-01-LEP-2, Geneva, 1996.

[12] *LHC Design Report, V.1: the LHC Main Ring*, CERN-

2004-003-V-1, Geneva, 2004.
[13] M. Pasini et al., *A SC Upgrade for the REX-ISOLDE Accelerator at CERN*, MOP028, LINAC 2008.
[14] P. Darriulat et al., *Study of the Surface Resistance of Superconducting Niobium Films at* 1.5 GHz, Physica C 316, 153188 (1999).
[15] A. Anders, *Structure Zone Diagram Including Plasma-Based Deposition and Ion Etching*, Thin Solid Films 518, 40874090 (2010).
[16] S. Bauer et al., *Production of Nb/Cu Sputtered Superconducting Cavities for LHC*, WEP016, SRF 1999.
[17] S. Aull et al., *On the Understanding of Q-Slope of Niobium Thin Films*, TUBA03, SRF 2015.
[18] S. Aull, *The Pathway to High Performance Superconducting Thin Films for RF Applications*, PhD Thesis, to be published.
[19] A.-M. Valente-Feliciano et al., *Material Quality & SRF Performance of Nb Films Grown on Cu via ECR Plasma Energetic Condensation*, TUPB029, SRF 2015.
[20] T. Junginger et al., *Extension of the Measurement Capabilities of the Quadrupole Resonator*, Rev Sci Instrum 83, (2012).
[21] G. Rosaz, *A15 Materials Thin Films and HiPIMS Progress at CERN for SRF Cavities*, EuCARD-2 3rd Annual WP12 Meeting, 2016.
[22] S. Aull and G. Rosaz *Measurement Report of the Cavity M5.3*, EDMS 1758468, 2017.
[23] S. Posen and M. Liepe, *RF Test Results of the First Nb_3Sn Cavities Coated at Cornell*, TUO087, SRF 2013.
[24] D. Hall and M. Liepe, *Current Peak Performance of* 1.3 GHz *Single-Cell Nb_3Sn Cavities Coated at Cornell with Associated Sample Surface Analysis*, Thin Film Workshop 2016
[25] G. Catelani and J. Sethna, *Temperature Dependence of the Superheating Field for Superconductors in the High-κ London Limit*, Phys Rev B. 78 224509, 2008.
[26] J. E. Mueller et al., *FCC HOM Power*, FCC Note, 2017, to be published.
[27] J. E. Mueller et al., *FCC HOM-Coupled Bunch Stability*, FCC Note, 2017, to be published.
[28] N. Schwerg et al., *FCC-ee: Interrelationships and Limits*, eeFACT2016, 2016.
[29] L. Tavian, *Private communication*, 2017.